Faster-Than-Nyquist signaling

A Thesis

submitted by

AKANSH JAIN

in partial fulfilment of the requirements

for the award of the degree of

BACHELOR AND MASTER OF TECHNOLOGY

DEPARTMENT OF ELECTRICAL ENGINEERING
INDIAN INSTITUTE OF TECHNOLOGY MADRAS.

5th May 2019

THESIS CERTIFICATE

This is to certify that the thesis titled **FASTER-THAN-NYQUIST signaling**, submitted by **Akansh Jain**, to the Indian Institute of Technology, Madras, for the award of the degree of **Bachelor and Master of Technology**, is a bona fide record of the research work done by him under our supervision. The contents of this thesis, in full or in parts, have not been submitted to any other Institute or University for the award of any degree or diploma.

Dr. David Koilpillai
Research Guide
Professor
Dept. of Electrical Engineering
IIT-Madras, 600036
Place: Chennai
Date: $5^{\mathbf{th}}$ May 2019

ACKNOWLEDGEMENTS

First and foremost, I express my sincere gratitude to my Research Guide, Prof. David Koilpillai, for his consistent guidance, motivation and support for my the research work. I would also like to thank him for providing wonderful and unique opportunities for my growth. I have learned a lot from him as a researcher as well as a professional.

I would also like to thank my co-guide Prof. Nambi Seshadri for nurturing and advising. His incites on the problems have been a huge help in solving them. Our weekly meetings facilitated me in learning how to solve research problems. It was a pleasure working with him.

I thank Sathwik Chadaga for his help in my research work as well his help in submitting the research paper. He has been a second pair of eyes throughout my DDP research.

I would like to thank my fellow researchers Mr. Pranav Opal, Mr. Neeraj Sharma, Mr. Tushar Golani, Mr. Swaminath M, Narendra Deconda, Shishir G, Romil Sonigra and Ashutosh Nikam for creating an interesting, cheerful and proactive research environment. I will never forget the lab discussions and tea breaks.

I express my gratitude to beloved my parents Mr. Rajesh Jain, Mrs. Varsha Jain and my brother Rishvik Jain for their constant support. My special thanks to Shri Sanjay bhaiya ji Morena for his guidance and wisdom. At last I thank the Almighty and his divine blessings.

ABSTRACT

KEYWORDS: FTN; OFDM; Single Carrier; Precoding; SVD; Inversion Precoding; MLSE; Nyquist Theorem

Faster-Than-Nyquist (FTN) Signaling is a non-orthogonal transmission scheme which violates the Nyquist zero-ISI criterion providing higher throughput and better spectral efficiency than a Nyquist transmission scheme. This comes with a cost of higher transceiver complexity. In this thesis, we focus on understanding pulse shapes and their inter-symbol-interference (ISI) and show that, under certain conditions on pulse shapes and τ (time acceleration factor), the ISI can be avoided completely with the help of precoding. This leads to a symbol-by-symbol detection. Further, we extend this idea to Orthogonal Frequency Division Multiplexing (OFDM) FTN systems and show that, under certain conditions, the average performance of OFDM system reaches that of a Nyquist system. Finally, simulation results of the performance of precoded and non-precoded single carrier and OFDM FTN systems are compared to a Nyquist system.

TABLE OF CONTENTS

LIST OF FIGURES

ABBREVIATIONS

AWGN	Analog White Gaussian Noise
BER	Bit Error Rate
BPSK	Binary phase shift Keying
CQI	Channel Quality Index
DFE	Decision Feedback Equalizer
DFT	Discrete Fourier Transform
DTFT	Discrete Time Fourier Transform
FFT	Fast Fourier Transform
FTN	Faster Than Nyquist
GMD	Geometric Mean Decomposition
GTMH	G To Minus Half
IDFT	Inverse Discrete Fourier Transform
IFFT	Inverse Fast Fourier Transform
i.i.d.	Independent and Identically Distributed
ISI	Inter Symbol Interference
MLSE	Maximum Likelihood Sequence Estimation
MMSE	Minimum Mean Square Error
OFDM	Orthogonal Frequency Division Multiplexing
PSD	Power Spectral Density
QAM	Quadrature Amplitude Modulation
RC	Raised Cosine
SRRC	Square Root Raised Cosine
SVD	Singular Value Decomposition
tri	Triangle

NOTATION

$b[n]$	Transmit bits
$g_{TX}(t)$	Transmit pulse
T_s	Symbol period or symbol duration
$g_{RX}(t)$	Matched filter pulse
$g_C(t)$	Channel filter
$X(f)$	Fourier transform of $x(t)$
τ	Acceleration factor
τ_{Mazo}	Mazo's limit on acceleration factor
α	Roll-off factor for the SRRC pulse
$g_{SRRC}(t)$	SRRC pulse
$g_{RC}(t)$	Raised cosine pulse
$E[,]$	Expected value operator
σ	Standard deviation
$a[n]$	symbols after modulation
η	White Gaussian noise
η'	Colored noise
$X(e^{j\omega})$	DTFT of $x[n]$
$\mathcal{H}_{RC}(f)$	Fourier transform of $h_{RC}(t)$
$\mathbb{Z}^+$	Set of all positive integers
$H_{tri}[i]$	i^{th} DFT coefficient of $h_{tri}[n]$

CHAPTER 1

INTRODUCTION

In a modern digital communication system, the information bits are transmitted by mapping them them to symbols in the (I,Q) space (e.g. M-QAM) [1]. These symbols are passed through a pulse shaping filter to obtain a continuous-time waveform. This waveform is up-converted and transmitted through the antenna. The pulse shaping ensures that the transmit signal is bandlimited, but it does not introduce ISI. Nyquist and Shannon formulated the Nyquist zero-ISI criterion which serves as the basis of all modern digital communication systems. The pulse should satisfy the Nyquist criterion for the continuous-time waveform to be ISI-free.

1.1 Prerequisite

Linear modulation is the technique of fundamental importance for communication over bandlimited channels. The complex baseband transmitted waveform for linear modulation can be written as

$$u(t) = \sum_{n} b[n] g_{TX}(t - nT_s) \tag{1.1}$$

Here $b[n]$ are the transmitted symbols taking values in a constellation. The modulating pulse $g_{TX}(t)$ is a fixed baseband waveform. The symbol rate, or baud rate is $1/T_s$, and T_s is the symbol interval.

Typically, a linearly modulated system is designed so as to avoid intersymbol interference at the receiver, assuming an ideal channel.

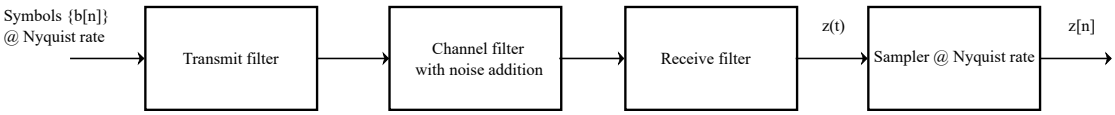

Figure 1.1: The block diagram representing Nyquist system

From Figure, the noiseless signal at the output of the receive filter is given by

$$z(t) = \sum_{n} b[n]x(t - nT_s) \tag{1.2}$$

where

$$x(t) = (g_{TX} * g_C * g_{RX})(t) \tag{1.3}$$

$x(t)$ is the overall response of the system to a single symbol. The Nyquist citerion ensures that $z(nT_s) = b[n]$ as given below.

Nyquist criterion for ISI avoidance:

Inter-symbol-interference can be avoided in the symbol-spaced samples, i.e., $z(nT_s) = b[n]$ for all n if,

$$x(mT_s) = \delta_{m0} = \begin{cases} 1, & m = 0 \\ 0, & m \neq 0 \end{cases} \tag{1.4}$$

Letting $X(f)$ denote the Fourier Transform of $x(t)$, the preceding condition can be equivalently written as

$$1/T_s \sum_{k=-\infty}^{k=\infty} X(f + \frac{k}{T_s}) = 1 \text{ for all } f \tag{1.5}$$

Most of the wireless communication technologies use raised cosine pulses for transmission as they are practical to implement compared to the sinc pulse or any other pulse shape for that matter, and they have a configurable excess bandwidth.

This rate is called the Nyquist rate. If the pulses are transmitted at this rate there is no ISI and the adjacent pulses are orthogonal to each other. If the symbols are transmitted above than this rate, orthogonal pulses will not be orthogonal and this introduces ISI. During pulse shaping, if symbols are spaced by T_s, Nyquist criterion ensures that there is no ISI. Such a system is called a Nyquist system. In recent years, transmitting the symbols faster than T_s has attracted attention. This technique is called the Faster-Than-Nyquist (FTN) Signaling. In FTN, pulse shaping is done with a pulse that is Nyquist with respect to T_s, but the symbols are spaced with a time period of τT_s where $\tau < 1$. The factor τ is called the time acceleration factor. This violates the Nyquist criterion with respect to τT_s and hence introduces ISI. This necessitates a complex transceiver

structure which is capable of mitigating ISI introduced by FTN signaling.

1.2 Focus of the Thesis

FTN is some of the more attractive ideas in terms of increasing the spectral efficiency. FTN helps to reach higher throughput by violating the Nyquist zero ISI criteria. Due to the violation of the zero ISI criteria, we have inherent ISI in the system. We focus on understanding the ISI and noise coloration present in FTN systems and analyzing the BER performance of Nyquist systems with traditional MLSE based decoders. We shift our focus to techniques which can help mitigate ISI. Precoding as a tool is used to mitigate ISI with the objective of doing symbol by symbol detection. Conditions on pulse shapes and acceleration factor (τ) are derived for which complete ISI mitigation is possible and BER performance of Nyquist systems is achieved. This is done with the help of precoding, specifically inversion based precoding. The derivation of condition for invertibility of the channel is derived in a very intuitive manner. Similar analysis can be done for any other pulse shape. For single carrier systems, we have focused on the SRRC pulse and for the OFDM systems, we have taken the rectangular pulse.

CHAPTER 2

LITERATURE SURVEY

In this chapter, we are going to discuss a survey on literature in FTN signaling. Initially, we will start with some early papers on FTN and then we discuss some recent papers.

In the early 1950s and 1960s, most of the communication advancements were published in the field of FTN. A Lot of findings were published but none of them had concrete results. In 1975 Mazo's work in the field of FTN played a significant role [2]. Mazo and Landau showed that if the acceleration factor τ is greater than τ_{Mazo} there is no decrease in the minimum distance in the transmitted waveforms [2, 3]. This result implied that if the minimum distance in the waveforms doesn't decrease then the probability of bit error doesn't increase.

There were many claims by researchers that data cannot be transmitted at a rate faster than the Nyquist rate. Tufts derived an analytical framework for FTN signaling with an MMSE equalizer and showed that it is possible to send data faster than Nyquist rate in short busts [4]. Few results were shown in the field by reducing system bandwidth slightly below Nyquist bandwidth which effectively was like simulating FTN signaling [5]. It was shown that the signals can be decoded with not much of a difficulty.

Around the 1970s, Forney's worked on the framework proposed by Viterbi and showed that the Viterbi decoder can be used for ISI channels [6, 7]. After some time Foschini studied the feasibility of FTN with certain modulation schemes like binary and QAM modulation [8]. But most of them were dropped as due to a large number of ISI taps in FTN the decoder complexity was very high for larger modulation schemes.

In the 1990s some Wang and Lee showed some significant improvements in the transmit filter and used a white and matched filter at the receiver [9].

In recent years some significant work is done by John B. Anderson and Fredrik Rusek. They showed the major benefits of the FTN signaling [10]. The major work shown is that the capacity of FTN systems for a finite alphabet is significantly higher than that of the orthogonal signaling schemes [11, 12].

In the work by Young Geon Etal, They examine the asymptotical optimality of binary FTN signaling [13]. They show that capacity can be achieved by using a transmit pulse which results in the same PSD as the water filling solution. To counter the issue of large ISI length ideas like MMSE channel shortening with MLSE equalizers were proposed [14]. It was shown that there is a trade-off between receiver complexity and performance.

Ideas like automatic trellis generation for Nyquist systems was also proposed [15] and it was shown that with certain constraints on channel length an automatic trellis can be generated. Mohamed G.El-Barbary et al discussed the performance of Simplified faster than Nyquist transceivers [16]. They presented results on Non-orthogonal OFDM which is like Faster than Nyquist signaling but in frequency. They used modified IDFT function and based on channel CQI discussed the use of adaptive non-orthogonality ratio.

Shoran Li et al proposed the use of different pulse shapes so as to get some gain over the traditional SRRC pulse [17]. They use Gaussian pulse and extended Gaussian function and show gains over the SRRC pulse. Different types of liner precoding techniques such as Singular Value Decomposition (SVD), G-to-Minus-Half (GTMH) and Cholesky Decomposition were proposed [18, 19]. It was shown that Cholesky Decomposition and GTMH precoding performed better than the SVD precoding at the cost of broadening the signal spectrum. Some improvements on GTMH precoding were also proposed. This gave a slight improvement in performance [20].

A frequency domain precoding technique was proposed which performed much better than the time domain GTMH and SVD precoding techniques. This frequency domain precoding allowed symbol-by-symbol detection at the receiver [16, 21]. The precoding based on matrix decomposition was also explored. Geometric mean decomposition (GMD) was shown to perform much better than DFE [18].

In this thesis, we build upon the previous work and analyze the pulse shapes closely and study the effect of ISI. We look at the performance of the MLSE receiver with constrained channel length. The major focus is on the analysis of pulse shapes and to derive the constraints on pulse shapes to reach Nyquist BER performance for a single carrier as well as OFDM systems. We also simulate the FTN system with whitening and precoding to achieve the Nyquist BER performance. We focus on showing the

conditions for channel inversion. The precoder used for the cases is a channel inversion based precoder.

CHAPTER 3

FTN signaling

In a Nyquist Communication system, at the transmitter, orthogonal pulses (orthogonal with respect to T_s) are transmitted at the rate $1/T_s$. The symbols can be independently received because of the orthogonality of pulse shapes. Symbols can be retrieved but using a matched filter which is matched to the transmit pulse shaping filter. But in case of faster than Nyquist signaling the same is not true. The pulse shapes are orthogonal with respect to time period T_s but are sent at an interval of τT_s ($\tau < 1$). For such a system the pulses sent are no longer orthogonal and give rise to intersymbol interference (ISI). This calls for a complex receiver structure.

We start by looking at the SRRC pulse. The following is the equation of SRRC pulse

$$g_{SRRC}(t) = \begin{cases} \frac{1}{T_s}(1+\alpha(\frac{4}{\pi}-1)), & t=0 \\ \frac{\alpha}{T_s\sqrt{2}}[(1+\frac{2}{\pi})\sin(\frac{\pi}{4\alpha}) + (1-\frac{2}{\pi})\cos(\frac{\pi}{4\alpha})] & t=\pm\frac{T_s}{4\alpha} \\ \frac{1}{T_s}\frac{\sin(\pi\frac{t}{T_s}(1-\alpha))+4\alpha\frac{t}{T_s}\cos(\pi\frac{t}{T_s}(1+\alpha))}{\pi\frac{t}{T_s}(1-(4\alpha\frac{t}{T_s})^2)} & otherwise \end{cases} \tag{3.1}$$

where, α is the roll-off factor. SRRC pulse is shown in the figure 3.1

The pulse for the n^{th} symbol in case of a faster than Nyquist system with acceleration factor τ ($\tau < 1$) is given as follows

$$g^n_{SRRC}(t) = g_{SRRC}(t - n\tau T_s) \tag{3.2}$$

3.1 Premise of FTN signaling

In FTN systems to get a discrete time system model, we use a matched filter similar to the one used in the Nyquist system. For the SRRC pulse, the matched filter is the same

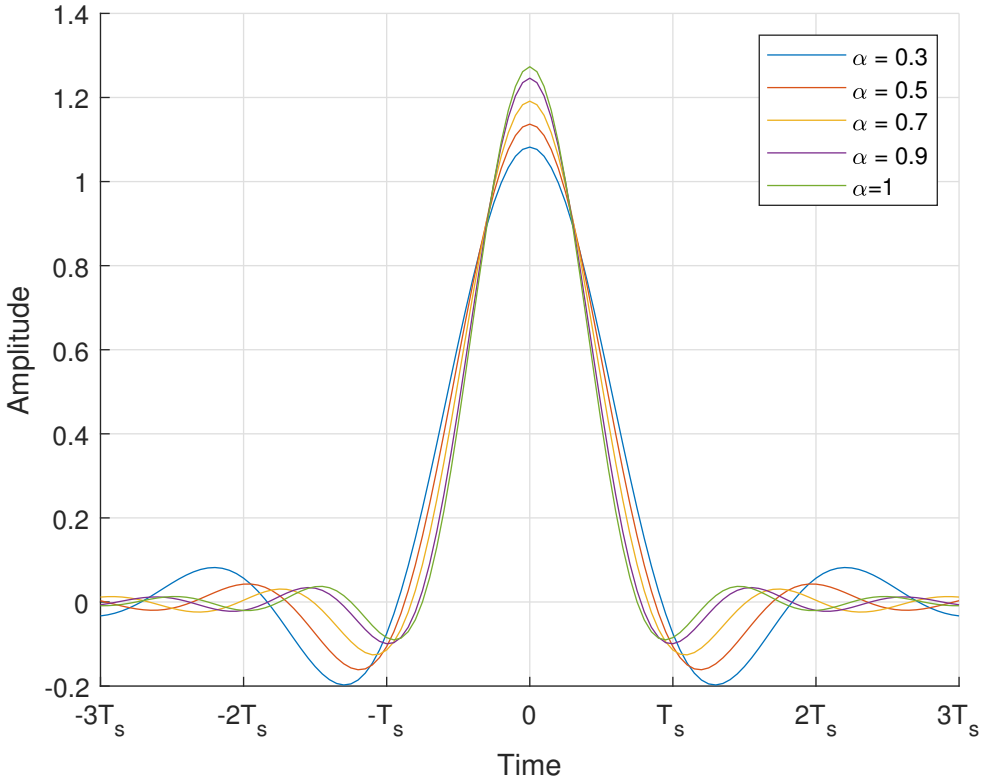

Figure 3.1: The SRRC pulse in time domain for different values of roll off α

as the transmit pulse. The received signal is passed through the matched filter and then sampled at a rate of $1/(\tau T_s)$ to obtain a discrete time model.

$$y_n = \langle r(t), g^n_{SRRC}(t)\rangle|_{\tau T} = \sum_{m=1}^{N} a_m \langle g^m_{SRRC}(t), g^n_{SRRC}(t)\rangle + \langle \eta'(t), g^n_{SRRC}(t)\rangle \quad n = 1, \ldots, N \tag{3.3}$$

This equation in discrete time simplifies to

$$y = Ga + \eta' \tag{3.4}$$

where,

$$G_{m,n} = \langle g^m_{SRRC}(t), g^n_{SRRC}(t)\rangle = g_{RC}((m-n)\tau T_s) \tag{3.5}$$

and $g_{RC}(t)$ is given as

$$g_{RC}(t) = \begin{cases} \frac{\pi}{4T_s}\frac{\sin(\frac{\pi}{2\alpha})}{\frac{\pi}{2\alpha}}, & t = \pm\frac{T_s}{2\alpha} \\ \frac{1}{T_s}\frac{\sin(\frac{\pi t}{T_s})}{\frac{\pi t}{T_s}}\frac{\cos(\frac{\pi\alpha t}{T_s})}{1-(\frac{2\alpha t}{T_s})^2} & otherwise \end{cases} \tag{3.6}$$

where, α is the roll-off factor. Figure 3.2 shows the RC pulse in time domain for different values of roll off α.

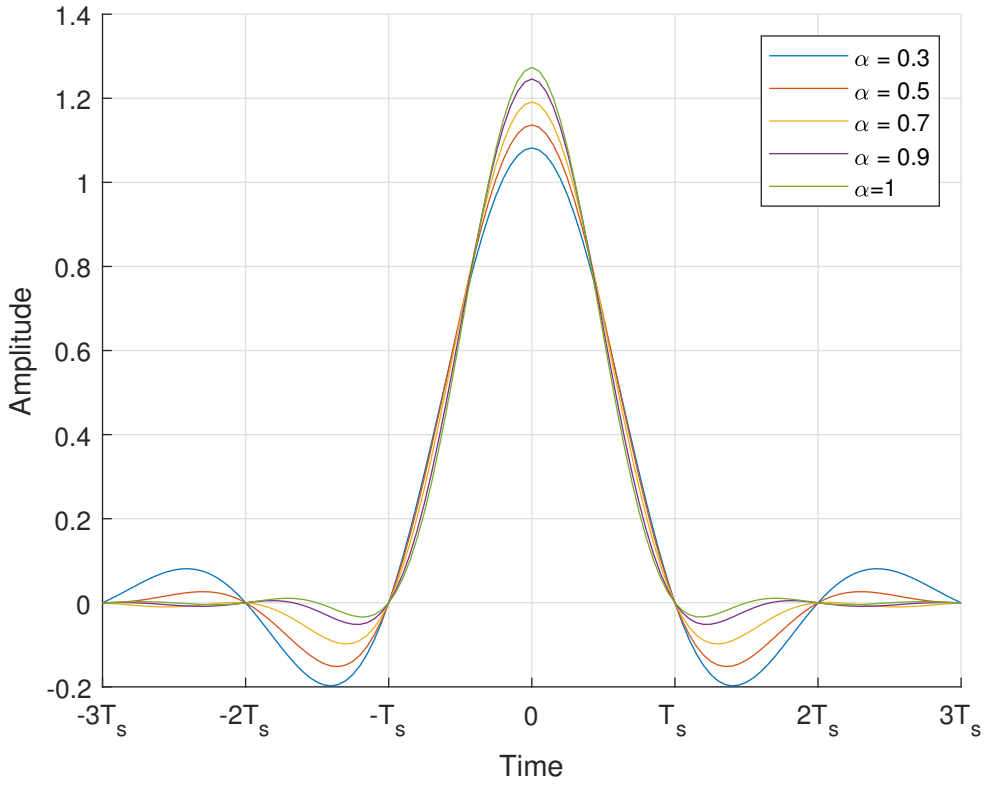

Figure 3.2: The RC pulse in time domain for different values of roll off α

G is matrix thus formed is a Toeplitz, Gram matrix. In the orthogonal Nyquist case G was diagonal and the noise was i.i.d. Gaussian distributed vector. The optimal Maximum-likelihood estimation was equivalent to a symbol by symbol detection.

In the case of FTN, G is not a diagonal matrix and the noise is no longer white Gaussian. This case introduces ISI depending on the value of τ and pulse shape. The noise is still zero mean and the covariance is calculated as follows

$$Cov(\eta'_m, \eta'_n) = E[\eta'_m, \eta'_n] = \sigma^2 G_{m,n} \tag{3.7}$$

Hence the Co-variance matrix of the noise is G. The overall τT_s spaced discrete time channel is as follows

In the figure 3.3, all channels are normalized to unit energy. As the value of τ reduces the length of the channel increases.

3.2 Solving ML estimation

Let's Simplify the equation for ML estimation by assuming G is an invertible matrix. It is shown in subsequent chapters that under certain constraints on the pulse shape and acceleration factor τ, G matrix can be proved to be invertible.

On assuming that invertibility of G, the ML estimation is simplified is as follows

$$Ga + \eta' = y \tag{3.8}$$

$$a + G^{-1} + \eta' = G^{-1}y \tag{3.9}$$

$$a + v = z \tag{3.10}$$

where, $z = G^{-1}y$ and $v \sim \mathcal{N}(0, \sigma^2 G^{-1})$. Using ML estimation theory $z \sim \mathcal{N}(a, \sigma^2 G^{-1})$ and the probability of z given a is as follows

$$\mathcal{P}(z|a) = \Big(\frac{1}{2\sigma^2\pi}\Big)^{N/2} \frac{1}{\sqrt{\det(G^{-1})}} e^{-\frac{1}{2\sigma^2}(z-a)^T G(z-a)} \tag{3.11}$$

To maximize the probability of we need to minimize $(z-a)^T G(z-a)$. This becomes a quadratic program.

$$\min_a (z-a)^T G(z-a)$$
$$s.t. \quad a \in \mathbf{S}^n$$

where, $\mathbf{S}$ belongs to the constellation or symbol space of transmission. This problem

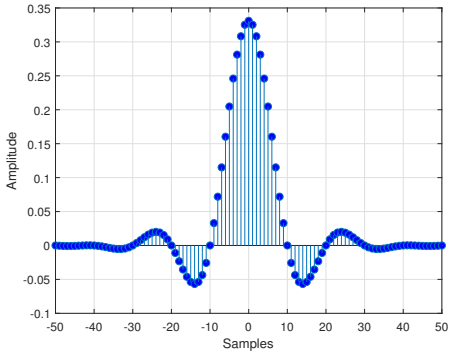

(a) $\tau = 0.1$

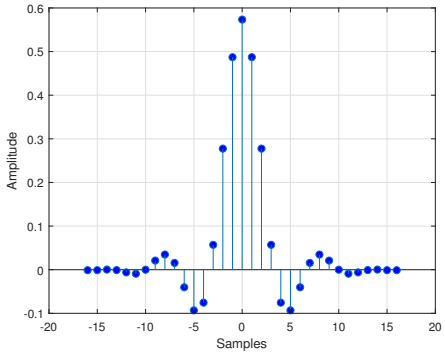

(b) $\tau = 0.3$

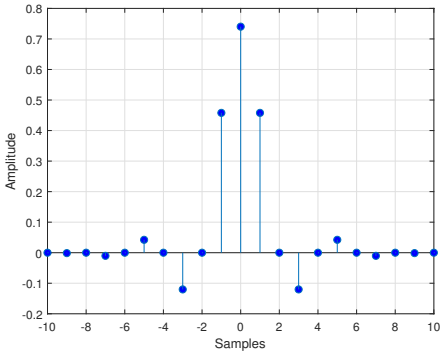

(c) $\tau = 0.5$

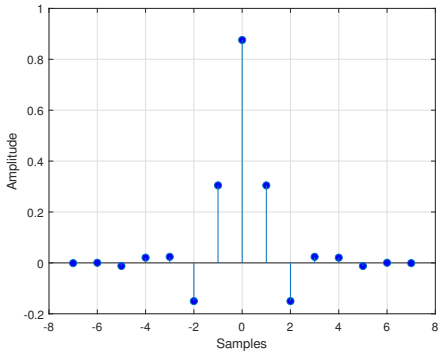

(d) $\tau = 0.7$

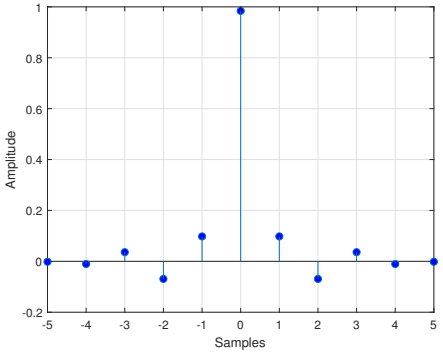

(e) $\tau = 0.9$

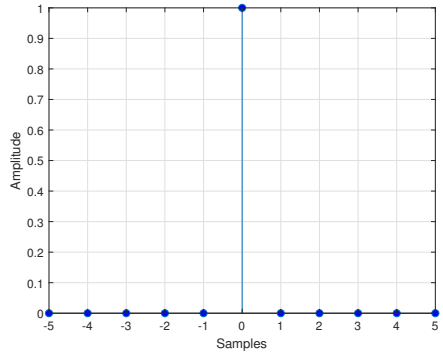

(f) $\tau = 1$

Figure 3.3: τT_s spaced Discrete time channel for different values of τ

is an NP-hard problem as the size of G increases. This implies that the complexity of solving this will be exponential.

In subsequent chapter, we propose methods to solve this problem by using different techniques.

CHAPTER 4

FTN signaling with MLSE

In this chapter, we discuss the methods to solve the problem by analyzing the ISI and then focusing on the whitening and other aspects of the FTN digital communication system.

4.1 Characterization of ISI and Spectrum Analysis

In this section, we look at the spectrum for the transmit pulse of the FTN system as well as the spectrum of the received waveform. We will also discuss the eye diagram and look at the effect of acceleration factor τ on the eye diagram and signal spectrum.

4.1.1 Signal Spectrum

After modulation, the modulated symbols are passed through a pulse shaping filter. The pulse shape used in the pulse shaping filter is orthogonal with respect to period T_s. The symbols are passed through the pulse shaping filter at a rate of $1/(\tau T_s)$. This waveform is passed through the AWGN channel. At the receiver, a matched filter is used which is matched to the transmit pulse shaping filter. After which a waveform is obtained. We analyze the spectrum at both the locations and look at the effect of τ. The pulse shaping filter used is an SRRC pulse with a roll-off factor α.

The transmit pulse is given as follows

$$r(t) = \sum_{n=1}^{N} a_n * g_{SRRC}(t - n\tau T_s) \tag{4.1}$$

where, a_n is the symbol at n^{th} time instant and τ is the acceleration factor. To plot the spectrum of the r(t) we normalize it by the number of symbols.

We plot the magnitude response of

$$R(f) = \mathcal{F}(r(t)/N) \tag{4.2}$$

To simplify this we use the shifting property of Fourier transform as follows

$$\mathcal{F}(g(t - t_0)) = e^{-i2\pi f t_0} G(f) \tag{4.3}$$

So the overall function $R(f)$ is given as follows

$$R(f) = \frac{1}{N} G_{SRRC}(f) \sum_{n=1}^{N} a_n e^{-i\pi\tau n f T_s} \tag{4.4}$$

As we can see from the above equation that the shape of $|R(f)|$ is upper bounded by $|G_{SRRC}(f)|$ by using Cauchy Schwartz inequality. Hence there is no bandwidth expansion w.r.t. acceleration factor τ. The figure below shows the normalized spectrum of transmit waveform $r(t)$ for different values of τ.

Figure 4.1: Transmit signal bandwidth for different values of τ

The similar analysis as above can be done for the received waveform after the

matched filtering. Let us call the waveform after match filtering as $y(t)$. The normalized Fourier transform of $y(t)$ can be given as follows

$$Y(f) = |G_{SRRC}(f)|^2 \frac{1}{N} \sum_{n=1}^{N} a_n e^{-i\pi\tau n f T_s} \tag{4.5}$$

hence the magnitude of Fourier transform of $y(t)$ i.e. $|Y(f)|$ is upper bounded by $|G_{SRRC}(f)|^2$. In this case, as well there is no bandwidth expansion w.r.t. τ. The figure below shows the normalized spectrum of received waveform after matched filtering i.e. $y(t)$ for different values of τ. The figure below shows the normalized spectrum of received waveform after matched filtering i.e. $y(t)$ for different values of τ.

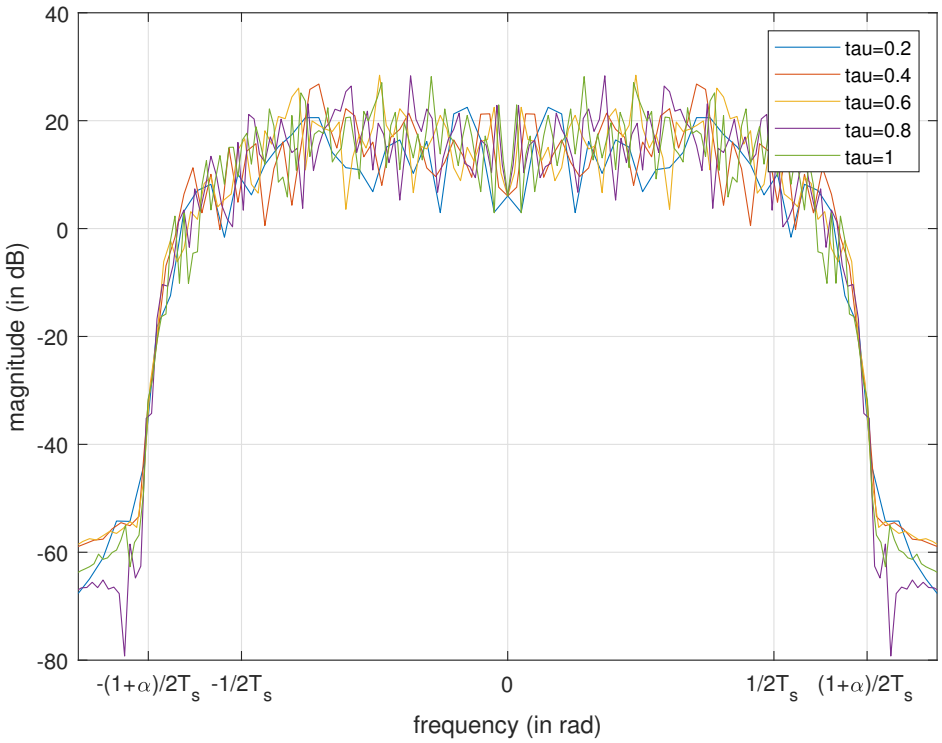

Figure 4.2: Received signal bandwidth after matched filtering for different values of τ

From the above explanation, we can see that the magnitude spectrum of $r(t)$ and $y(t)$ both are upper bounded by the pulse shape and not on the value of τ. Hence FTN doesn't expand the bandwidth of the transmitted waveform.

4.1.2 Eye Diagram

In this section, we analyze the effect of τ on eye-opening and eye-opening locations for the received waveform after the matched filtering. The timing locations at which the maximum eye opening occurs can be calculated by finding the time instances where the correlation is maximum which can be seen as below

$$y(t) = (\sum_{n=1}^{N} a_n g_{SRRC}(t - n\tau Ts)) * g_{SRRC}(-t) \tag{4.6}$$

where $*$ means convolution. Here $g_{SRRC}(-t)$ is the matched filter which is convoluted with $r(t)$ to get $y(t)$. This gives rise to the correlation of $g_{SRRC}(t)$ with itself. This correlation is maximum when its argument is zero. Hence the sampling should take at intervals of τT_s. Hence the eye-opening will be seen at intervals of τT_s.

As the value of τ decreases, there is a significant increase in ISI. This will also be reflected in the eye diagram. The number of states in the eye diagram at the sampling intervals will increase as the value of τ decreases. For lower values of τ it will be difficult to see the eye openings at the sampling intervals.

The eye diagrams are shown for some values of τ in figure 4.3

From the eye diagrams in figure 4.3, we can infer that the eye openings are at intervals of τT_s. As the values of τ decreases the size of openings decreases. The decrease in eye openings results due to increase in ISI. In the next section we try and analyze the MLSE performance in presence of noise for different values of τ.

4.2 Performance of FTN with MLSE

In this section, we do simulations and study the effect of acceleration factor τ on the BER performance. The focus in this section is to understand noise coloration and how it affects the BER performance.

The setup for the simulation is give in figure 4.4

At the transmitter, the information bits are modulated to a symbol space. These symbols are then passed through a transmit pulse shaping filter. In these simulations

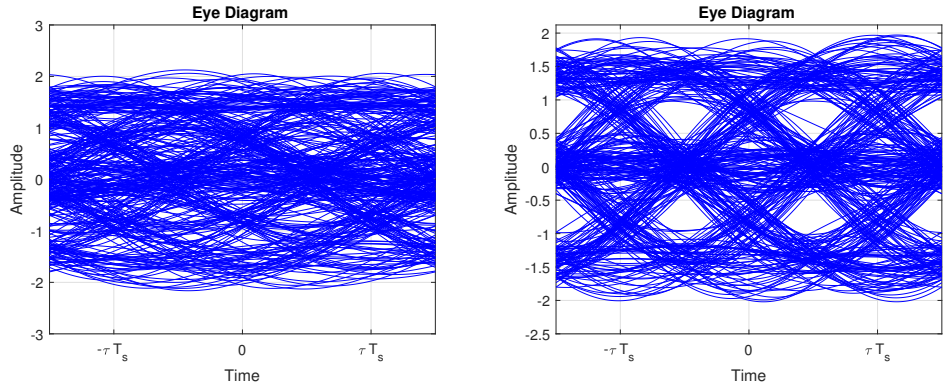

(a) $\tau = 0.5$ (b) $\tau = 0.6$

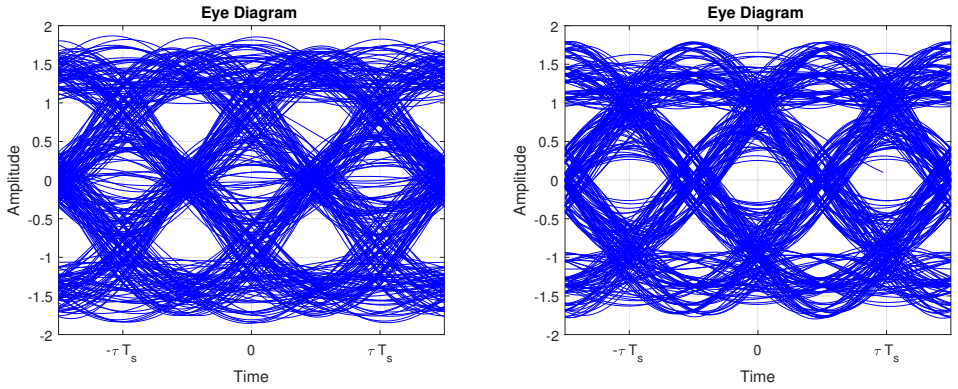

(c) $\tau = 0.7$ (d) $\tau = 0.8$

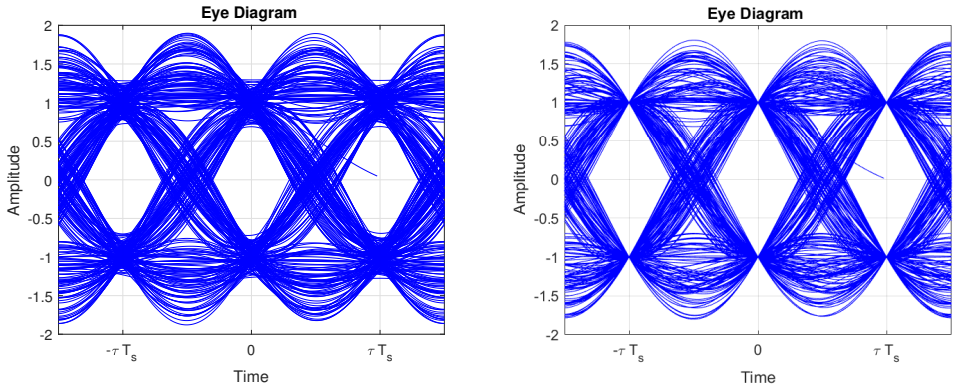

(e) $\tau = 0.9$ (f) $\tau = 1$

Figure 4.3: Eye diagram for different values of τ

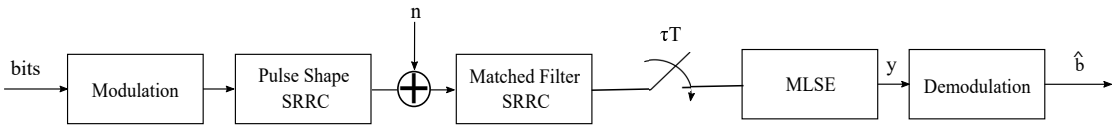

Figure 4.4: Block diagram for FTN with MLSE

the transmit pulse shaping filter used is SRRC pulse with a roll-off factor $\alpha = 0.35$. The symbols are input to the matched filter at intervals τT_s. The output waveform from the transmit pulse shaping filter is passed through an AWGN channel and noise is added at the receiver.

The waveform received is passed through a matched filter. This matched filter is matched to the transmit filter. The waveform obtained from the matched filter is sampled at an interval of τT_s. After sampling we get a discrete sequence $y[n]$. The sequence $y[n]$ is passed through MLSE. The MLSE is implemented using the Viterbi algorithm.

The ISI channel length increases as the value of τ decreases. The complexity of MLSE using Viterbi algorithm is exponential with ISI length. So because of the highly complex receiver, we limit the channel length to 15 taps. These 15 taps are calculated by sampling RC pulse at an interval of τT_s. The ISI is given by

$$h[n] = g_{RC}(t)|_{\tau T_s} = g_{RC}(n\tau T_s) \quad n \in \{-7, -6, \ldots, -1, 0, 1, \ldots 6, 7\} \tag{4.7}$$

The MLSE estimation is done and BER is calculated with $h[n]$ as channel input to MLSE. The modulation scheme chosen is BPSK. The BER performance of MLSE with the above-mentioned constraints is shown below.

The figure 4.5 shows that as the value of τ reduces the MLSE BER performance reduces.

4.2.1 Issues with above simulation

In the above simulations, we put some constraints on the channel ISI. To keep simulation complexity in check we limited the number of states in the Viterbi algorithm to 2^{14} for a BPSK scheme. But the validity of this approximation reduces as the value of τ reduces. The length of the ISI increases and the approximation of limiting the number of states is not valid. For low values of τ the number of states required for the Viterbi algorithm is very large and requires a highly complex receiver. To compensate for this issue some other algorithms like BCJR, M-BCJR, etc. can be implemented.

After passing through the matched filtering and sampling, the sampled data is directly fed to an MLSE algorithm. The noise just before the MLSE is colored as the

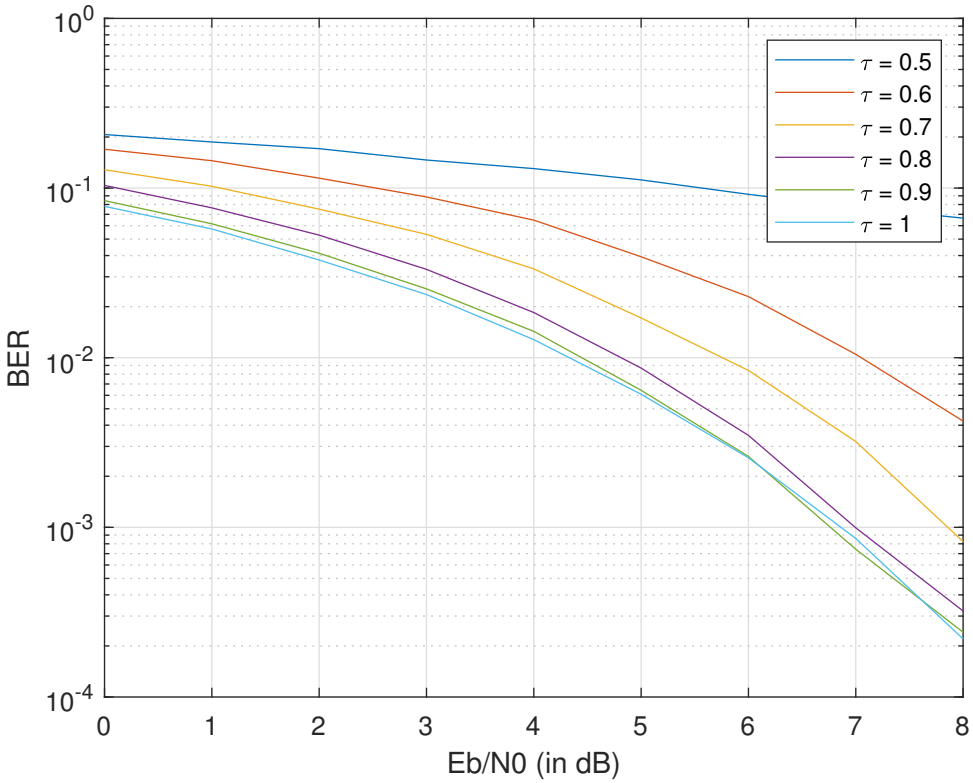

Figure 4.5: BER performance of FTN with MLSE

covariance of noise is given by $\sigma^2 G_{RC}$. G_{RC} is not a diagonal matrix for $\tau < 1$. As the noise is colored the MLSE via Viterbi algorithm is not the optimal estimation. In the next section, we will study the effect of noise coloration and channel dispersion and look at the BER performance of both under MLSE.

4.2.2 Noise Coloring Simulation

For this simulation we follow the following block diagram

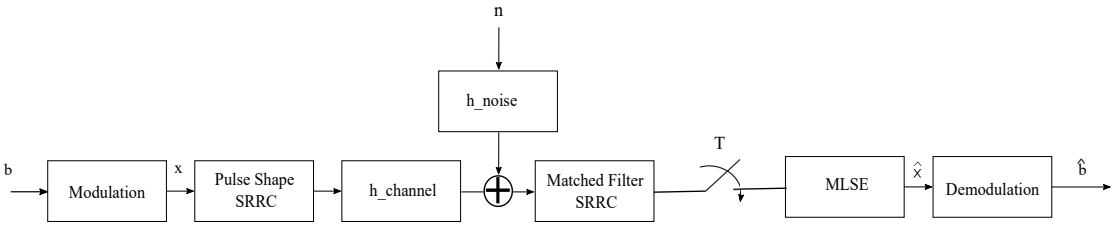

Figure 4.6: Noise coloration block diagram

the bits are modulated to BPSK modulation and then Nyquist SRRC pulse (roll off $\alpha = 0.35$) shaping is done. Waveform is then passed through a normalized channel of the form $h_{ch}[n] = \frac{1}{\sqrt{1+\gamma^2}}(1 + \gamma z^{-1})$. For noise colouration a white Gaussian noise

is passed through a filter of the form $h_{noise}[n] = \frac{1}{\sqrt{1+\beta^2}}(1 + \beta z^{-1})$. this filter adds coloration to noise. The colored noise is added to the signal. The overall signal obtained is then passed through a matched filter. the Output of the matched filter is sampled and sent to MLSE. Then MLSE estimation is done at the receiver and the BER performance is plotted for multiple values of γ for a given value of noise coloration i.e. β. The BER curves are shown below

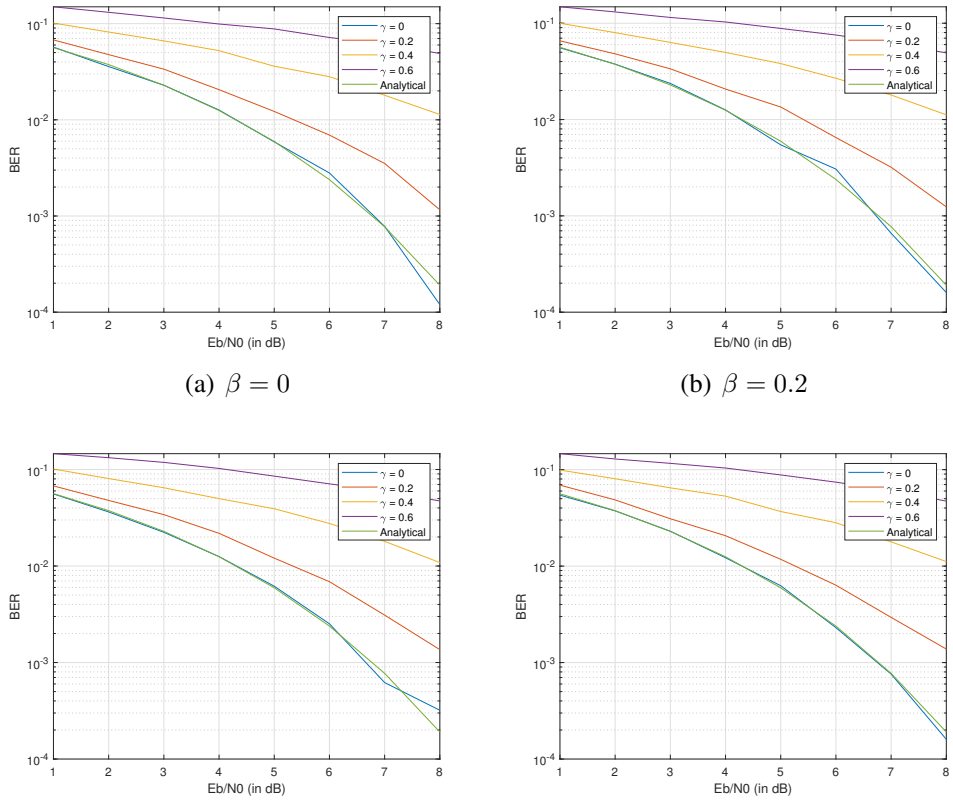

(a) $\beta = 0$ (b) $\beta = 0.2$

(c) $\beta = 0.4$ (d) $\beta = 0.6$

Figure 4.7: BER performance for different values of γ given a value of β

The BER performance is also plotted for multiple values of β given a value of γ. The plots are shown in figure 4.8

4.2.2.1 Effect of channel dispersion and noise coloration

The effect of channel dispersion can be seen clearly in all the figures [refer]. As the value of γ increases, the BER performance degrades significantly for all noise coloration.

On the other hand for a given value of channel dispersion, the effect of noise coloration is not very significant. We can see that with the increase in the value of β the

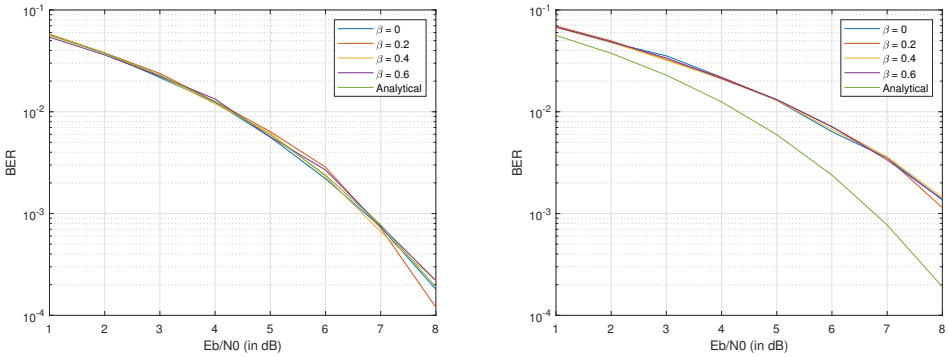

(a) $\gamma = 0$ (b) $\gamma = 0.2$

(c) $\gamma = 0.4$ (d) $\gamma = 0.6$

Figure 4.8: BER performance for different values of β given a value of γ

BER degradation is not very severe.

From the above observation, we can say that the effect of noise coloration is very minimal as compared to that of channel dispersion. In the next section, we explore a new matched filter which can eliminate noise coloration.

4.2.3 Rx Matched Filter

In this section, we explore a way to remove noise coloration. Instead of using a filter matched to the transmit SRRC filter (orthogonal with T_s), we use a matched filter with SRRC pulse which is orthogonal with τT_s. Thus the covariance matrix of the noise calculated in this case is diagonal. Hence the noise, in this case, becomes white. The block diagram of the setup is shown in figure 4.9

In this case, we simulate the BER performance and the results are shown in figure 4.10 for some values of τ close to 1.

From the curves above we can see that the matched filter matched to τT_s performs

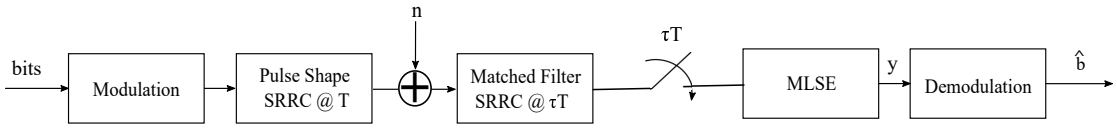

Figure 4.9: Block diagram for τT_s matched filter at receiver

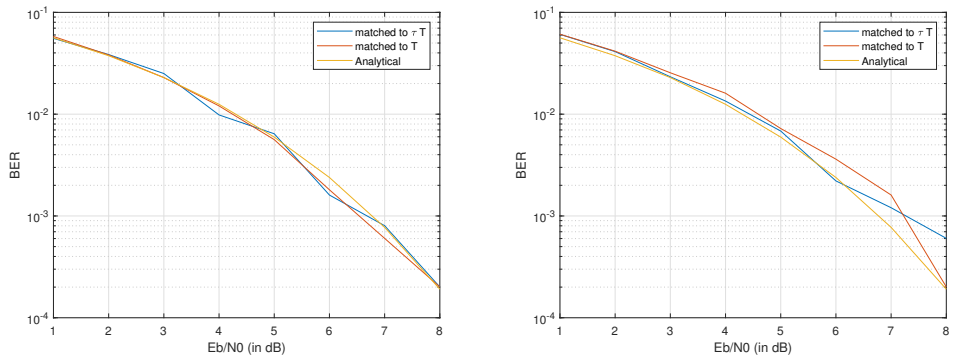

(a) $\tau = 0.95$

(b) $\tau = 0.9$

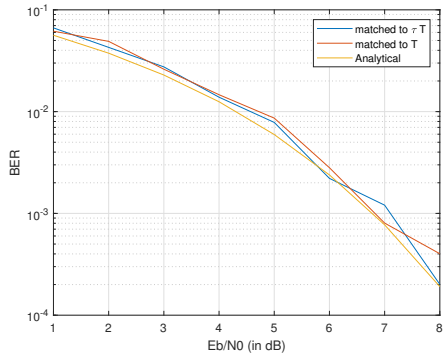

(c) $\tau = 0.85$

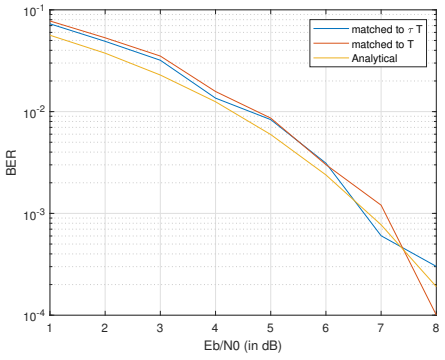

(d) $\tau = 0.8$

Figure 4.10: BER performance of τT_s matched received filter for τ close to 1 compared to T_s matched received filter

slightly better than the filter matched to T_s. But as the value of τ decreases the BER performance degrades. The main factor in BER performance degradation is ISI.

CHAPTER 5

Precoding

As seen in the previous chapter, ISI is the key factor in BER performance degradation. The ISI present in the system was handled by use of an MLSE based Viterbi decoder. But due to the large ISI length, the complexity of the optimal decoder was very high.

Precoding is one of the effective ways to mitigate ISI. With the help of proper precoding techniques, we can do a symbol by symbol detection and the high receiver complexity can be eliminated. Precoding also provides flexibility in power allocation and can be very useful in OFDM like multicarrier systems.

In this chapter, we explore precoding techniques like SVD and inversion based precoding and derive the framework for it.

5.1 SVD based precoding

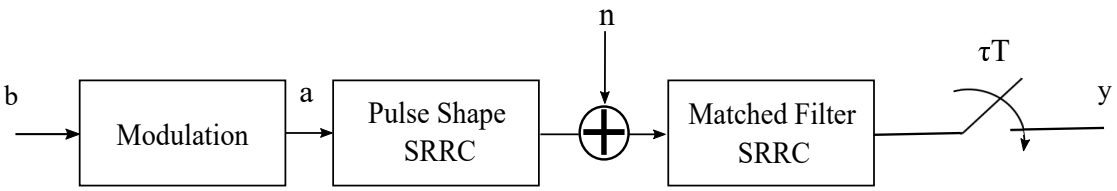

Figure 5.1: Block diagram of a single carrier system

From the block diagram, the equation for $y[n]$ can be written as follows

$$G_{RC}a + \eta' = y \tag{5.1}$$

where, η' is a colored noise with mean zero and covariance matrix $\sigma^2 G_{RC}$. As the G matrix is symmetric the SVD can be written in the following form.

$$G_{RC} = U\Sigma U^* \tag{5.2}$$

Using the decomposition in 5.2 equation in 5.1 can be simplified as follows

$$U\Sigma U^* a + U\sqrt{\Sigma}U^*\eta = y \tag{5.3}$$

Instead of transmitting symbols we pre-code them with a precoding matrix as follows

$$\hat{a} = Ua \tag{5.4}$$

Now at the receiver, we multiply the received symbols by matrix U^*. the equations simplify as follows

$$U\Sigma U^*\hat{a} + U\sqrt{\Sigma}U^*\eta = y \tag{5.5}$$

$$U\Sigma a + U\sqrt{\Sigma}\hat{\eta} = y \tag{5.6}$$

where, $\hat{\eta}$ is also white Gaussian noise as multiplication by a unitary matrix doesn't change the covariance. Now both sides are multiplied by U^* and the simplification is as follows

$$U^*(U\Sigma a + U\sqrt{\Sigma}\hat{\eta}) = U^*(y) \tag{5.7}$$

$$\Sigma a + \sqrt{\Sigma}\eta = \hat{y} \tag{5.8}$$

$$\Sigma a + w = \hat{y} \tag{5.9}$$

where, Σ is a diagonal matrix and w is a white Gaussian noise with zero mean and co-variance $\sigma^2\Sigma$. The overall system can be represented as follows

$$\Sigma a + w = \hat{y} \tag{5.10}$$

Now from the above equation as Σ is a diagonal matrix so symbol by symbol detection is possible. The BER performance depends on the values of Σ_i corresponding to that symbols. If the value of $\Sigma_i = 0$ then the symbol a_i cannot be recovered. The

overall block diagram is given as follows

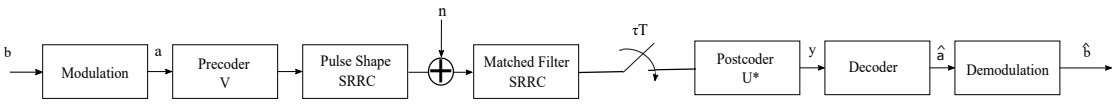

Figure 5.2: Block diagram of a single carrier system with SVD precoder

5.2 Inversion based precoding

In this section, we focus on inversion based precoding to achieve the BER performance of a Nyquist system. In the case of SVD based Precoding the system performance depends on the value of Σ_i. So to remove that also we try an inversion based precoding technique where we try to invert the effect of ISI so that symbol by symbol detection can be done and the Nyquist BER performance can be achieved. To be able to check for invertibility of the ISI we derive the conditions on pulse shapes and acceleration factor τ in the subsequent sections. If the channel is invertible then $\Sigma_i \neq 0 \quad \forall i$. In this case we precode it with inverse of the channel. The precoding is mentioned in depth in section 5.3.

5.3 Conditions on channel/pulse shape for perfect recovery

In this section, we try to derive the conditions on pulse shape and acceleration factor τ so that the channel can be inverted. We do the same for both Single carrier systems as well as OFDM systems. We also look at whitening the noise and provide expressions for noise whitening filter. In cases where channel inversion is not possible we implement a precoding filter which tries to reduce channel ISI so the MLSE estimation can be used.

5.3.1 Single Carrier

The FTN baseband single-carrier communication system is represented by the block diagram shown in figure 5.3. At the transmitter, the modulated symbols are passed at a rate of τT_s ($\tau < 1$) through a pulse shaping filter that is Nyquist with respect to T_s. The

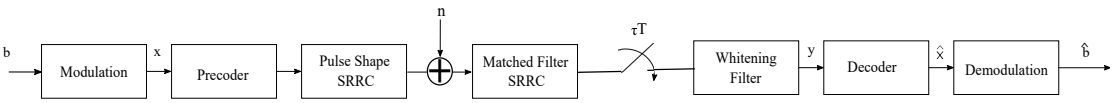

Figure 5.3: The block diagram representing single-carrier FTN system.

FTN waveform thus obtained is transmitted through an AWGN channel. At the receiver, the received waveform is passed through a filter that is matched to the transmit pulse shaping filter. The output of the filter is sampled at τT_s to get discrete time samples.

The overall system can be represented as

$$y[n] = h_{RC}[n] * x[n] + \eta'[n] \tag{5.11}$$

where, $h_{RC}[n]$ is RC pulse sampled at τT_s, η' is the colored noise due to the FTN signaling and $*$ represents convolution. This can be represented in the matrix form as

$$\mathbf{y} = \mathbf{H_{RC}}\mathbf{x} + \eta' \tag{5.12}$$

where, $\mathbf{x}$ and $\mathbf{y}$ are transmitted and received sequences respectively, η' is the corresponding colored noise and $\mathbf{H_{RC}}$ is a circulant matrix formed by the channel $h_{RC}[n]$.

To estimate the transmit sequence $\hat{\mathbf{x}}$ symbol-by-symbol from received sequence $\mathbf{y}$, $\mathbf{H_{RC}}$ should be invertible. It is invertible when its eigenvalues are non-zero. Since $\mathbf{H_{RC}}$ is a circulant matrix, its eigenvalues are given by the DFT coefficients of $h_{RC}[n]$. Hence, the analysis of DFT coefficients of $h_{RC}[n]$ is done below.

The continuous time Fourier transform $\mathcal{H}_{RC}(f)$ of RC pulse is bandlimited by $(1+\alpha)/2T_s$ where, α is the roll-off factor i.e. $\mathcal{H}_{RC}(f) = 0$ for $|f| > (1+\alpha)/2T_s$. As the RC pulse is sampled at τT_s, the DTFT $H_{RC}(e^{j\omega})$ is given by

$$H_{RC}(e^{j\omega}) = \frac{1}{\tau T_s} \sum_{k=-\infty}^{\infty} \mathcal{H}_{RC}\left(\frac{1}{2\pi}\left(\frac{\omega}{\tau T_s} - \frac{2\pi k}{\tau T_s}\right)\right). \tag{5.13}$$

If the DTFT $H_{RC}(e^{j\omega})$ is non-zero for all frequencies ω, the DFT coefficients are non-zero. To satisfy this condition, the passbands or the transition bands of adjacent copies should overlap as shown in figure 5.4. In this case, the overall response $H_{RC}(e^{j\omega})$ is non-zero for all frequencies ω i.e. $H_{RC}(e^{j\omega}) > 0, \forall\omega$.

If the values of τ are very small, the adjacent copies are non-overlapping as shown

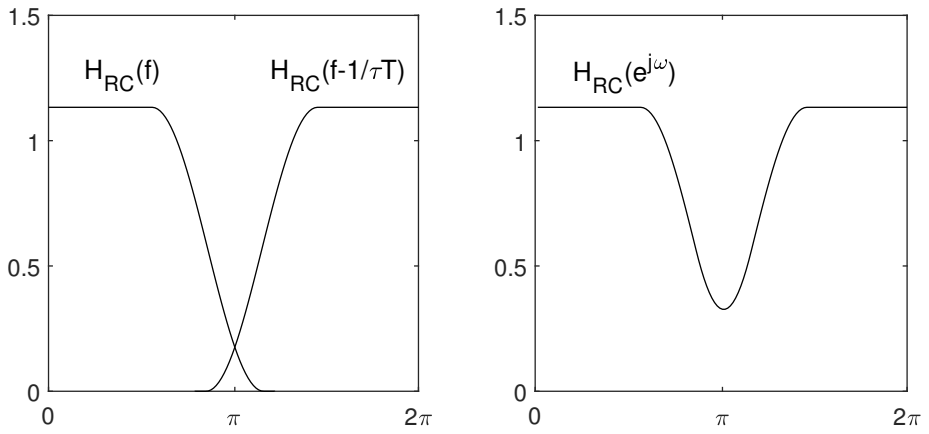

Figure 5.4: The DTFT $H_{RC}(e^{j\omega})$ when the adjacent copies of the CTFT $\mathcal{H}_{RC}(f)$ are overlapping. In this case, the overall response is non-zero for all frequencies.

in figure 5.5. In this case, there are certain frequencies ω where the overall response is zero i.e. $H_{RC}(e^{j\omega}) = 0$, for some ω.

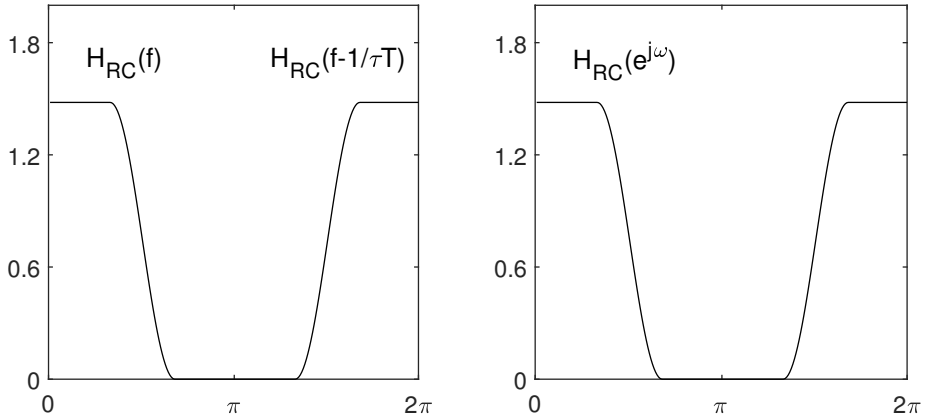

Figure 5.5: The DTFT $H_{RC}(e^{j\omega})$ when the adjacent copies of the CTFT $\mathcal{H}_{RC}(f)$ are non-overlapping. In this case, there are certain frequencies ω where the overall response is zero.

In order to ensure that the adjacent copies are overlapping, τ should satisfy the following condition.

$$\frac{1+\alpha}{2T_s} > \frac{1}{\tau T_s} - \frac{1+\alpha}{2T_s},$$

$$(1+\alpha)\tau > 1. \tag{5.14}$$

If the condition in (5.14) is satisfied, the DFT coefficients of $h_{RC}[n]$ are non-zero. This implies that the circulant matrix $\mathbf{H_{RC}}$ in (5.12) has all non-zero eigenvalues and

hence is invertible. So, symbol-by-symbol detection can be done with the help of precoding.

In the following sub-sections, the precoding and whitening in single-carrier FTN system model is discussed. Sub-section 5.3.1.1 considers the case when (5.14) is satisfied and Sub-section 5.3.1.2 considers the case when (5.14) is not satisfied.

5.3.1.1 Single-carrier FTN with $(1+\alpha)\tau > 1$

If the condition in (5.14) is satisfied, the DTFT $H_{RC}(e^{j\omega}) > 0$, $\forall\omega$. So, $h_{RC}[n]$ does not have any zeros on the unit circle. As $h_{RC}[n]$ is real, symmetric and has no zeros on the unit circle, it can be spectral factorized as

$$H_{RC}(z) = \gamma^2 H_{in}(z) H_{in}^*(1/z^*) \tag{5.15}$$

where, $H_{in}(z)$ is the monic and causal factor of $H_{RC}(z)$. Now, the noise can be whitened by a whitening filter given by $H_W(z) = 1/\left(\gamma H_{in}^*(1/z^*)\right)$. Along with whitening, the system model with rate τT is

$$y[n] = \gamma h_{in}[n] * x[n] + \eta[n] \tag{5.16}$$

where, $h_{in}[n]$ is the monic and causal IDFT of $H_{in}(z)$ from (5.15), and $\eta[n]$ is white noise. Now, this system can further be simplified by precoding the transmit sequence using a filter $1/\gamma H_{in}(z)$. Finally, with both whitening and precoding, the overall system model is as follows

$$y[n] = x[n] + \eta[n]. \tag{5.17}$$

Symbol-by-symbol detection can be done on this overall model.

5.3.1.2 Single-carrier FTN with $(1+\alpha)\tau < 1$

If the condition in (5.14) is not satisfied, the DTFT $H_{RC}(e^{j\omega}) = 0$, for some ω. So, $h_{RC}[n]$ has some zeros on the unit circle. Hence, the spectral factorization of $H_{RC}(z)$ is done as follows

$$H_{RC}(z) = \gamma^2 H_{in}(z) H_{on}(z) H_{out}(z)$$

$$= \gamma^2 H_{in}(z) H_{on}(z) H_{in}^*(1/z^*) \tag{5.18}$$

where, the factors $H_{in}(z)$, $H_{on}(z)$ and $H_{in}^*(1/z^*)$ contain all zeros inside, on and outside the unit circle respectively. As complete whitening is not possible, unlike the previous case, partial whitening is done as $H_W(z) = 1/\gamma H_{in}^*(1/z^*)$. A precoding filter given by $1/\gamma H_{in}(z)$ is used. Finally, with both whitening and precoding, the overall system model is as follows

$$y[n] = h_{on}[n] * x[n] + \eta[n] \tag{5.19}$$

where, $h_{on}[n]$ is the IDFT of $H_{on}(z)$ and has zeros on the unit circle. Symbol-by-symbol detection cannot be used to estimate the complete sequence $\mathbf{x}$ in this case. Hence, a Maximum likelihood sequence estimation is employed.

5.3.2 Multicarrier (OFDM)

The FTN baseband multi-carrier OFDM communication system is represented by the block diagram shown in figure 5.6. At the transmitter, after the N-point IFFT operation and parallel-to-serial conversion, the symbols are passed at a rate of τT_s ($\tau < 1$) through a rectangular pulse shaping filter. The pulse shaping has a response of $rect(t/T_s)$. At the receiver, the matched filter has a response of $rect(t/T_s)$. The output of the matched filter is then sampled at rate τT_s making the overall response a triangular pulse $h_{tri}(t)$ sampled at τT_s.

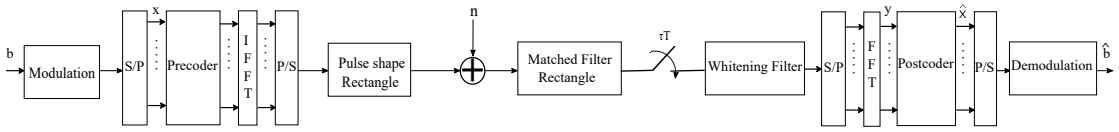

Figure 5.6: The block diagram representing OFDM FTN system.

The overall system model of OFDM is given by

$$y[i] = H_{tri}[i]x[i] + \eta'[i] \quad i = 0, \ldots, N-1 \tag{5.20}$$

where, $H_{tri}[i]$ is the i-th coefficient of N-point DFT of $h_{tri}(t)|_{\tau T_s}$ and $\eta'[i]$ is the colored noise. It should be noted that each value of i corresponds to each sub-carrier of OFDM. To estimate $x[i]$ from $y[i]$, none of the $H_{tri}[i]$ should be equal to zero i.e. none of the

DFT coefficients of $h_{tri}(t)|_{\tau T_s}$ should be zero. The continuous time Fourier transform of $h_{tri}(t)$ is given below

$$\mathcal{H}_{tri}(f) = \left(\frac{\sin(\pi f T_s)}{\pi f T_s}\right)^2. \tag{5.21}$$

Now, the DTFT $H_{tri}(e^{j\omega})$ is

$$H_{tri}(e^{j\omega}) = \frac{1}{\tau T_s} \sum_{k=-\infty}^{\infty} \mathcal{H}_{tri}\left(\frac{1}{2\pi}\left(\frac{\omega}{\tau T_s} - \frac{2\pi k}{\tau T_s}\right)\right)$$

$$= \frac{1}{\tau T_s} \sum_{k=-\infty}^{\infty} \left(\frac{\sin((\omega - 2\pi k)/2\tau)}{(\omega - 2\pi k)/2\tau}\right)^2. \tag{5.22}$$

The value of $H_{tri}(e^{j\omega})$ will be zero at some frequencies ω if all the copies in the summation are zero at ω. This situation occurs when

$$(\omega - 2\pi k)/2\tau = \pi l \quad \forall l \in \mathbb{Z} \setminus \{0\}. \tag{5.23}$$

Noting that $0 < \tau < 1$, this condition simplifies to

$$\tau = 1/l \quad \forall l \in \mathbb{Z}^+ \setminus \{1\}. \tag{5.24}$$

So, the condition for $H_{tri}(e^{j\omega})$ to be non-zero is

$$\tau \neq 1/l \quad \forall l \in \mathbb{Z}^+ \setminus \{1\}. \tag{5.25}$$

If the condition (5.25) is satisfied, then $H_{tri}(e^{j\omega})$ is non-zero for all frequencies ω.

In figure 5.7(a), the channel does not satisfy the condition in 5.25 and has some frequencies ω where $H_{tri}(e^{j\omega})$ goes to zero. The sub-carriers corresponding to those frequencies have $H_{tri}[i] = 0$. Thus, those sub-carriers cannot be used to transmit symbols. In figure 5.7(b), the channel satisfies condition in 5.25 and is non-zero for all frequencies ω. Precoding can be used in this case to utilize all the sub-carriers and reach the BER performance of a Nyquist system.

In the following sub-sections, the precoding and whitening in OFDM FTN system model is discussed. Sub-section 5.3.2.1 considers the case when equation 5.25 is satis-

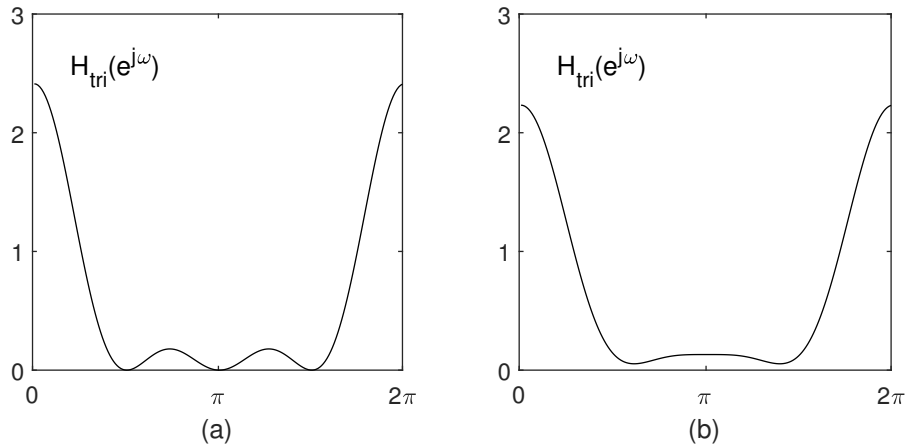

Figure 5.7: (a) The channel does not satisfy the condition (5.25) and is zero for some frequencies. (b) The channel satisfies condition (5.25) and is non-zero for all frequencies.

fied and Sub-section 5.3.2.2 considers the case when equation 5.25 is not satisfied.

5.3.2.1 OFDM FTN with $\tau \neq 1/l$

In this case, $H_{tri}[i]$ from (5.20) is ensured to be non-zero. So, $H_{tri}(z)$ can be spectral factorized as

$$H_{tri}(z) = \gamma^2 H_{in}(z) H_{in}^*(1/z^*). \tag{5.26}$$

As the noise is colored, the whitening filter is derived from the above equation as

$$H_w(z) = 1/\gamma H_{in}^*(1/z^*). \tag{5.27}$$

The system model along with whitening becomes

$$y[i] = \gamma H_{in}[i] x[i] + \eta[i] \quad i = 0, \ldots, N-1 \tag{5.28}$$

where, $\eta[i]$ is white noise and $H_{in}[i]$ is the DFT of $h_{in}[n]$ the monic and causal factor of $h_{tri}(t)|_{\tau T_s}$.

Since $H_{in}[i]$ is ensured to be non-zero, $x[i]$ can be precoded as $\tilde{x}[i] = x[i]/\gamma H_{in}[i]$. The overall system with both whitening and precoding is

$$y[i] = x[i] + \eta[i] \quad i = 0, \ldots, N-1. \tag{5.29}$$

The system model for each sub-carrier in (5.29) is equivalent to a Nyquist system model. So the performance of OFDM FTN system with precoding and whitening reaches that of a Nyquist system.

5.3.2.2 OFDM FTN with $\tau = 1/l$

In this case, $H_{tri}[i]$ is zero for some sub-carriers i. Hence the spectral factorization of $H_{tri}(z)$ is done as

$$H_{tri}(z) = \gamma^2 H_{in}(z) H_{on}(z) H_{out}(z)$$

$$= \gamma^2 H_{in}(z) H_{on}(z) H_{in}^*(1/z^*) \tag{5.30}$$

where, the factors $H_{in}(z)$, $H_{on}(z)$ and $H_{in}^*(1/z^*)$ contain all zeros inside, on and outside the unit circle respectively. A whitening filter is implemented as $H_W(z) = 1/\gamma H_{in}^*(1/z^*)$. The precoding is done as $\tilde{x}[i] = x[i]/\gamma H_{in}[i]$. The overall model after whitening and precoding is

$$y[i] = H_{on}[i]x[i] + \eta[i] \quad i = 0, \ldots, N-1 \tag{5.31}$$

where, $\eta[i]$ is white noise and $H_{on}[i]$ are the DFT coefficients of $h_{on}[n]$, the inverse z-transform of $H_{on}(z)$. In this system model, $H_{on}[i]$ is zero for some sub-carriers i and those sub-carriers cannot be used to transmit symbols. Hence, the average BER performance over all the sub-carriers is not close to that of a Nyquist system.

CHAPTER 6

SIMULATION

In this chapter, we describe the setup for simulation and present the results of simulations. The theory for the simulations is discussed in the previous chapter. The simulations are done for both single carrier and multi-carrier(OFDM) systems.

6.1 Single-Carrier FTN System

The simulation of single carrier FTN system was performed using BPSK modulation. The pulse used in this case was square-root-raised-cosine (SRRC) pulse with a roll-off factor $\alpha = 0.35$. The BER curves obtained without and with precoding are shown in Fig. 6.1(a) and Fig. 6.1(b) respectively. In the simulations without precoding, MLSE was used at the receiver. In the simulations with precoding, MLSE was used in cases where symbol-by-symbol detection was not possible. All the results are compared against the Nyquist system (i.e. the system with $\tau = 1$).

From (5.14), the condition on τ for symbol-by-symbol detection is $\tau > 1/(1+\alpha)$ which gives $\tau > 0.7407$ for $\alpha = 0.35$. This implies that for values of $\tau > 0.7407$, it is possible to reach the BER performance of Nyquist systems if precoding is used.

Figure 6.1(a) shows the BER curves for the case where the symbols were transmitted without precoding. A whitening filter was used at the receiver as discussed in Section 5.3.1. MLSE detection was used as precoding is not done. As the value of τ decreases, the amount of ISI increases and hence the complexity of MLSE increases. But for this simulation, the maximum number of states in MLSE trellis was kept fixed. So, the BER performance degrades as τ decreases. Further for the value of $\tau < 0.7407$, only partial whitening can be done as the zeros of $h_{RC}[n]$ are on the unit circle (Section 5.3.1.2). Since MLSE is optimal only when the noise is white, the BER performance for $\tau = 0.7$ is further degraded.

The eye diagrams of the received signal in the case without precoding are shown in figure 6.2

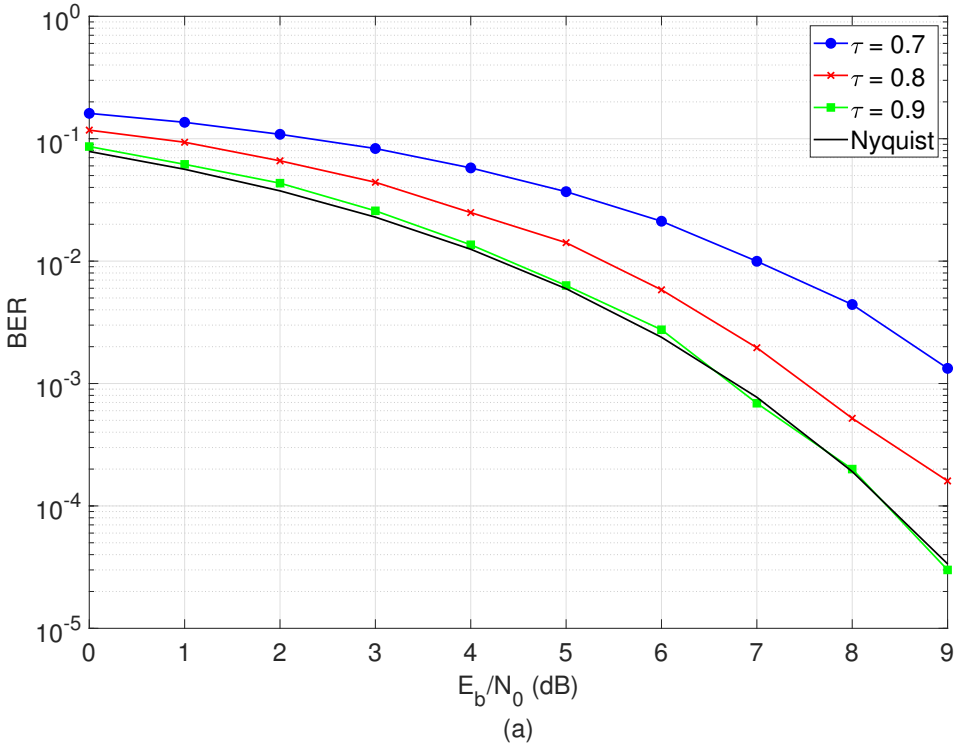

Figure 6.1: (a) Simulation results for single carrier FTN system with BPSK modulation using SRRC pulse (roll-off 0.35) without precoding. (b) Simulation results for single carrier FTN system with BPSK modulation using SRRC pulse (roll-off 0.35) with precoding.

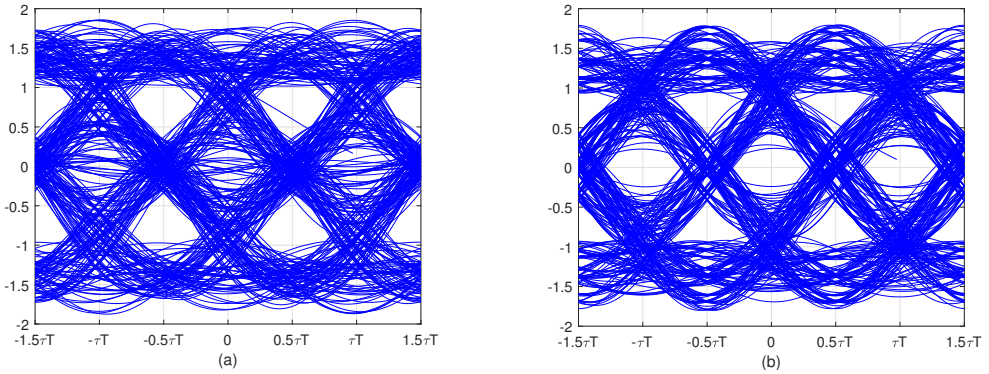

Figure 6.2: (a) Eye diagram for $\tau = 0.7$ without precoding. (b) Eye diagram for $\tau = 0.8$ without precoding.

There is no clear eye opening in both cases as precoding is not done and symbol-by-symbol detection is not possible.

Figure 6.1(b) shows the BER curves for the case where the symbols were transmitted with precoding and a whitening filter was used at the receiver. For $\tau > 0.7407$, the ISI channel $h_{RC}[n]$ has no zeros on the unit circle. So, the channel was inverted using precoding and symbol-by-symbol detection was done. Hence the BER performance of the system for these values of τ reaches that of a Nyquist system. But for $\tau < 0.7407$, the ISI channel $h_{RC}[n]$ has zeros on the unit circle and symbol-by-symbol detection and whitening cannot be done. So, MLSE was used at the receiver and partial whitening was done as discussed in Section 5.3.1.2. As noise is not completely white, MLSE is not optimal. Hence, the performance of the system in this case ($\tau = 0.7$) does not reach that of a Nyquist system.

The eye diagrams of the received signal in the case with precoding are shown in figure 6.3.

For $\tau = 0.7$, there is no clear eye opening as ISI is present even with precoding. But for $\tau = 0.8$, there is clear eye opening as precoding enables symbol-by-symbol detection.

6.2 Multi-Carrier OFDM FTN System

The simulation of OFDM FTN system was performed using BPSK modulation. The pulse shape used in this case was rectangular. The BER curves obtained without and

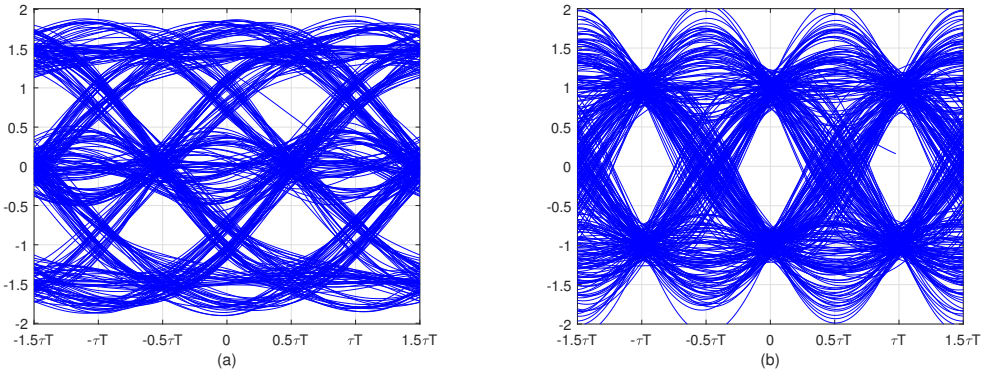

Figure 6.3: (a) Eye diagram for $\tau = 0.7$ with precoding. (b) Eye diagram for $\tau = 0.8$ with precoding.

with precoding are shown in Fig. 6.4(a) and Fig. 6.4(b) respectively.

From (5.25), the condition for all the sub-carrier channels to be non-zero is $\tau \neq 1/l \quad \forall l \in \mathbb{Z}^+ \setminus \{1\}$ i.e. $\tau \neq 1/2, 1/3, \ldots$. For these values of τ, it is possible to reach the BER performance of a Nyquist system with precoding as discussed in Section 5.3.2.1. For other values of τ, symbols on certain sub-carriers cannot be estimated, hence the average BER performance of this system does not reach that of a Nyquist system as discussed in Section 5.3.2.2.

Figure 6.4(a) shows the BER curves for the case where symbols were transmitted without precoding and a single tap equalizer was used at the receiver. The channel response $H_{tri}[i]$ of each sub-carrier i is given by the DFT coefficients of $h_{tri}(t)|_{\tau T_s}$ as shown in (5.22). As the value of τ decreases, the separation between adjacent copies in Fig. 5.7 increases. As a result, some of the sub-carriers experience very small values of $H_{tri}[i]$ and the BER performance of these sub-carriers degrade. Hence, as the value of τ decreases, the average BER performance of the OFDM system degrades.

Figure 6.4(b) shows the BER curves for the case where symbols were transmitted with precoding. For the values of $\tau \neq 1/2$, the condition (5.25) is satisfied and hence, as discussed in Section 5.3.2.1, $H_{tri}[i] \neq 0$ for all sub-carriers. So, after precoding as $\tilde{x}[i] = x[i]/\gamma H_{in}[i]$, the overall system model for each sub-carrier (5.29) is the same as that of a Nyquist system. So, the performance of OFDM system when $\tau \neq 0.5$ reaches that of a Nyquist system. But for $\tau = 0.5$, as discussed in Section 5.3.2.2, there are some sub-carrier for which $H_{tri}[i] = 0$. The sub-carriers having $H_{on}[i] \neq 0$ reach the BER performance of a Nyquist system with precoding. But some of the sub-carriers

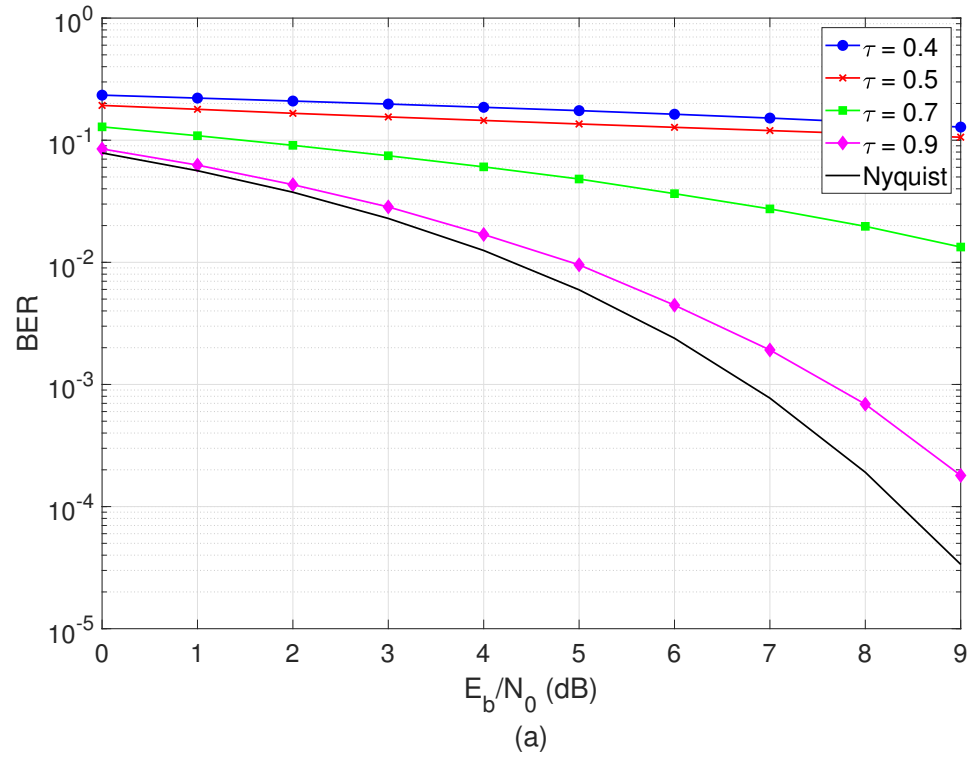

Figure 6.4: (a) Simulation results for OFDM FTN system with BPSK modulation using rectangular pulse without precoding. (b) Simulation results for OFDM FTN system with BPSK modulation using rectangular pulse with precoding.

that have $H_{on}[i] = 0$ cannot be used to transmit symbols. Hence, the average BER performance for $\tau = 0.5$ is worse compared to other values of τ (even $\tau = 0.4$).

CHAPTER 7

DISCUSSIONS

FTN signaling has a huge potential in terms of its higher capacity as compared to the Nyquist signaling scheme. Due to the large ISI length and noise coloration present in the FTN system the overall BER performance did not reach that of a Nyquist system. With the help of precoding, we showed that the performance of Nyquist system can be achieved under certain conditions on pulse shapes and acceleration factor τ. The higher sampling rate causes the sampled spectrum copies to spread apart. This causes the sampled signal spectrum to become zero for a certain set of frequencies. Hence, inversion based precoding is not possible.

In a single carrier system, the transmit pulse shaping filter and the received matched filter together form RC pulse. The FTN technique gains its benefit from the excess bandwidth of the RC pulse. For pulse shapes with excess bandwidth lower than the RC pulse, the conditions on time acceleration factor τ will be more stringent.

Rectangular pulses are used for OFDM systems in the 4G standards (LTE Adv). Hence, the OFDM FTN system was analyzed with a rectangular transmit pulse shaping filter. OFDM systems using pulses other than the rectangular pulse (possibly with a lower time-bandwidth product and better spectral confinement) can be analyzed in a similar fashion.

The BER performance of OFDM FTN system reaches that of a Nyquist system with the use of the proposed precoding scheme. As the value of τ decreases, more and more sub-carriers experience bad channel. So the channel inversion based precoding scheme discussed in this paper requires higher transmit power for those sub-carriers. This, in turn, results in an increase of PAPR of the OFDM FTN system. Instead, other schemes like water-filling can be explored. Also, techniques like choosing higher order modulation for good sub-carriers can be explored.

CHAPTER 8

KEY RESULTS and SUMMARY

The transceiver of FTN systems can become highly complex as the value of τ reduces. We simulated the BER performance of MLSE based Viterbi decoder for values of τ. It was seen that the BER performance degrades as the value of τ reduces. We showed that under certain conditions, simple precoding techniques can be used to mitigate ISI completely with the help of precoding. After complete mitigation of ISI, symbol-by-symbol detection can be done. In those cases, we showed that the BER performance can reach that of a Nyquist system in both single carrier and OFDM FTN systems. This comes with a cost of higher transmit power as we are packing more and more symbols in a given time period while keeping the average symbol energy same.

Single carrier systems with SRRC pulse shape with roll-off factor α as the transmit filter reach the Nyquist BER performance if the following Condition is satisfied

$$(1+\alpha)\tau > 1 \tag{8.1}$$

where, τ is the acceleration factor for the FTN system.

For OFDM systems with rectangular pulses the condition is as follows

$$\tau \neq \frac{1}{l} \quad l \in \mathbb{Z}^{+} \tag{8.2}$$

where,τ is the acceleration factor.

If the pulse shape satisfies the conditions mentioned above then inversion based precoding can be used to achieve Nyquist BER performance for the system.

The complete block structure is explained in the cases were 8.1 is satisfied as well as when condition 8.1 is not satisfied. The same is also done for the OFDM system based on condition 8.2.

CHAPTER 9

FUTURE WORK

FTN signaling schemes have a lot of avenues to explore. It is a relatively new area of research and a lot of stones unturned. Some of the areas that can be explored are as follows

- Implement and analyze a Deep learning based receiver and compare the BER performance with the MLSE based system.
- Use error coding schemes to get better BER performance
- Study the effect of precoding and analyze the BER performance with the maximum power constraint.
- Optimize the current precoding scheme to increase the capacity of the FTN system.
- Pulse shape can also be optimization for FTN systems to limit the ISI length. A similar analysis for condition on τ can be done.

REFERENCES

[1] Upamanyu Madhow. *Fundamentals of Digital Communication*. Cambridge University Press, South Asia, 2017.

[2] J. E. Mazo. Faster-than-nyquist signaling. *The Bell System Technical Journal*, 54(8):1451–1462, Oct 1975.

[3] J. E. Mazo and H. J. Landau. On the minimum distance problem for faster-than-nyquist signaling. *IEEE Transactions on Information Theory*, 34(6):1420–1427, Nov 1988.

[4] D. W. Tufts. Nyquist's problemâĂŤthe joint optimization of transmitter and receiver in pulse amplitude modulation. *Proceedings of the IEEE*, 53(3):248–259, March 1965.

[5] B. Saltzberg. Intersymbol interference error bounds with application to ideal bandlimited signaling. *IEEE Transactions on Information Theory*, 14(4):563–568, July 1968.

[6] G. D. Forney. The viterbi algorithm. *Proceedings of the IEEE*, 61(3):268–278, March 1973.

[7] G. Forney. Maximum-likelihood sequence estimation of digital sequences in the presence of intersymbol interference. *IEEE Transactions on Information Theory*, 18(3):363–378, May 1972.

[8] G. J. Foschini. Contrasting performance of faster binary signaling with qam. *AT T Bell Laboratories Technical Journal*, 63(8):1419–1445, Oct 1984.

[9] and. Practically realizable digital transmission significantly below the nyquist bandwidth. *IEEE Transactions on Communications*, 43(2/3/4):166–169, Feb 1995.

[10] J. B. Anderson, F. Rusek, and V. ÃŰwall. Faster-than-nyquist signaling. *Proceedings of the IEEE*, 101(8):1817–1830, Aug 2013.

[11] F. Rusek and J. B. Anderson. Constrained capacities for faster-than-nyquist signaling. *IEEE Transactions on Information Theory*, 55(2):764–775, Feb 2009.

[12] F. Rusek and J. B. Anderson. Cth04-1: On information rates for faster than nyquist signaling. In *IEEE Globecom 2006*, pages 1–5, Nov 2006.

[13] Y. G. Yoo and J. H. Cho. Asymptotic Optimality of Binary Faster-than-Nyquist Signaling. *IEEE Communications Letters*, 14(9):788–790, Sep. 2010.

[14] J. Fan, Y. Ren, Y. Zhang, and X. Luo. Mlse equalizer with channel shortening for faster-than-nyquist signaling. *IEEE Photonics Technology Letters*, 30(9):793–796, May 2018.

[15] D. Govindaraj and M. Bazdresch. Automatic trellis generation for demodulation of faster than nyquist signals. In *2017 IEEE Western New York Image and Signal Processing Workshop (WNYISPW)*, pages 1–5, Nov 2017.

[16] M. G. El-Barbary, F. A. Newagy, and I. M. Hafez. Performance of simplified faster-than-nyquist tranceiver. In *2016 7th International Conference on Information and Communication Systems (ICICS)*, pages 174–179, April 2016.

[17] S. Li, Z. Wu, and H. Che. Faster-than-nyquist system based on novel shaping waveforms. In *2016 Sixth International Conference on Instrumentation Measurement, Computer, Communication and Control (IMCCC)*, pages 461–464, July 2016.

[18] S. Nie, M. Guo, and Y. Shen. Precoding based on matrix decomposition for faster-than-nyquist signaling. In *2015 IEEE 5th International Conference on Electronics Information and Emergency Communication*, pages 194–197, May 2015.

[19] H. Wang, A. Liu, X. Liang, S. Peng, and K. Wang. Linear precoding for faster-than-nyquist signaling. In *2017 3rd IEEE International Conference on Computer and Communications (ICCC)*, pages 52–56, Dec 2017.

[20] Y. Zhang, J. Lei, and W. Liu. An improved gtmh precoding algorithm in faster-than-nyquist signaling system. In *2018 International Conference on Electronics Technology (ICET)*, pages 341–344, May 2018.

[21] X. Liang, A. Liu, K. Wang, Q. Zhang, and S. Peng. Symbol-by-symbol detection for faster-than-nyquist signaling aided with frequency-domain precoding. In *2016 6th International Conference on Electronics Information and Emergency Communication (ICEIEC)*, pages 14–17, June 2016.